ADVANCED ENERGY MATERIALS
www.advenergymat.de

Critical Role of Non-Fullerene Crystalline Domains in Stabilizing Charge Separation in Bulk Heterojunction Organic Solar Cells

Soyeong Jeong, Aniket Rana, Weidong Xu, Keren Ai, Rachel Catherine Kilbride, Yiwen Wang, Damin Lee, Pabitra Shakya Tuladhar, Hyojung Cha, and James Robert Durrant**

This study addresses the role of energetic offsets resulting from non-fullerene acceptor crystallization/aggregation in stabilizing charge separation in organic bulk heterojunction (BHJ) solar cells. Devices are fabricated using PM6 as electron donor and either IDIC or Y6 as acceptor, with blend ratios from 5:1 to 1:1. Reducing acceptor content significantly lowers device performance, most notably for initially higher performing PM6:Y6 BHJ's (from 14.31% to 0.95%) compared to PM6:IDIC (from 11.28% to 3.40%). Optical, optoelectronic, and morphological characterizations reveal that lower acceptor content PM6:Y6 devices exhibit suppressed acceptor aggregation/crystallinity, correlated with increased recombination losses and lower efficiency. Charge separation in optimal (1:1) PM6:Y6 devices is found to be stabilized by a LUMO level energetic offset between intermixed and pure, more crystalline, Y6 domains, driven by strong electronic interactions between Y6 molecules. In contrast, PM6:IDIC devices show minimal changes in energetics and recombination kinetics, aligning with their smaller performance decline, and consistent with IDIC's weaker electronic interactions. As such strong electronic interactions between Y6 molecules are concluded to provide an energetic stabilization of electrons in more aggregated/crystalline Y6 domains, suppressing charge recombination, and analogous to that observed for the highest performing fullerene acceptor PCBM.

1. Introduction

Non-fullerene acceptors (NFAs) based organic photovoltaic devices (OPVs) have achieved remarkable success, yielding power conversion efficiencies (PCEs) now approaching 21%, primarily attributed to optimized molecular structures, energy levels, and absorption spectra.[1–6] These high efficiencies are further supported by efficient charge separation with minimal energetic losses, contributing to both high short-circuit current densities (J_{SC}) and open circuit voltages (V_{OC}). Particularly the NFA Y6, which features an A–D–A'–D–A configuration, has attracted great attention for its high performance, correlated with strong molecular packing in solid films. This packing promotes substantial electronic coupling between adjacent Y6 molecules, facilitating exciton delocalization and creating an efficient 3D charge transport network, suggested to

S. Jeong, A. Rana[+], K. Ai, P. S. Tuladhar, J. R. Durrant
Department of Chemistry and Centre for Processable Electronics
Imperial College London
White City Campus
London W12 0BZ, UK
E-mail: j.durrant@imperial.ac.uk

W. Xu
Department of Chemical Engineering and Biotechnology
Office 1-03, Philippa Fawcett Drive, Cambridge CB3 0AS, UK

The ORCID identification number(s) for the author(s) of this article can be found under https://doi.org/10.1002/aenm.202501633

[+]Present address: Department of Engineering, Durham University, Durham DH13LE, UK

DOI: 10.1002/aenm.202501633

R. C. Kilbride
Department of Chemistry
University of Sheffield
Sheffield S3 7HF, UK

Y. Wang
School of Engineering and Materials Science
Queen Mary University of London
Mile End Road, London E1 4NS, UK

D. Lee, H. Cha
School of Energy Engineering
Kyungpook National University
Daegu 41566, Republic of Korea
E-mail: hcha@knu.ac.kr

J. R. Durrant
SPECIFIC
Faculty of Science and Engineering
Swansea University
Swansea SA1 8EN, UK

further enhance device performance.[7] While much of the focus has been on the importance of crystalline/aggregated, molecularly pure NFA phases within bulk heterojunction (BHJ) films, the further presence of molecularly mixed phases is both inevitable[8,9] and often advantageous for efficient device performance. These mixed phases increase the interfacial area for charge generation and form a continuous interpenetrating network of the donor (D) and acceptor (A) molecules, facilitating efficient charge transport.[10] In previous studies of BHJ films of donor polymers with the fullerene electron acceptor PCBM, it was reported that PCBM aggregation resulted in an increase in electron affinity, providing an additional energetic offset between molecular mixed and pure PCBM domains that facilitates the separation of free electron and holes.[11] Consequently, it is important to understand how NFA molecular design impacts upon whether an analogous energetic offset exists between molecular mixed and pure NFA domains, and how this impacts device PCE.

The behavior of charge carriers between mixed and pure phases remains rather poorly understood, particularly in recently developed NFA-based solar cells.[12] One strategy to adjust the proportion of mixed and pure domains is by varying the D:A ratio within the BHJ. Studies investigating the ratio of D to A provide not only fundamental insights into the role of mixed and pure domains but are also important for establishing composition and processing windows for commercial applications. In blends with high NFA content, NFA aggregation often predominates due to strong intermolecular interactions.[13,14] It has also been suggested that such aggregation can positively influence charge separation.[15] Additionally, low donor content polymer:NFA blends can be of particular interest due to their lower visible light absorption, making them suitable for OPV window applications.[16] For these reasons, we employ herein BHJ films with varying donor polymer:NFA ratios to explore the effects of pure and mixed domains on exciton behavior and free charge carrier generation and recombination. We then examine how these factors influence overall device performance.

In this study, we investigated BHJ films and solar cells comprising the donor polymer PM6 and two NFAs, IDIC and Y6 (see Figure S1, Supporting Information for chemical names and structures). These NFAs have been widely studied for their potential to achieve high performance in OPVs, with Y6 demonstrating stronger intermolecular couplings compared to IDIC, including those arising from its unusually high molecular quadrupole.[17–19] Recent ultrafast exciton annihilation measurements indicate that these NFAs exhibit diffusion lengths ranging from 15 to 40 nm, a significant advantage over fullerene acceptors, allowing excitons to traverse longer distances to reach a charge separation interface.[20,21] We examine the interplay between blend ratio and charge carrier densities, energetics, and recombination dynamics in order to identify the underlying mechanisms driving the variation in device performance across different blend ratios, employing a range of morphological, optical, and optoelectronic analyses.

2. Results and Discussion

To evaluate the performance of OPVs as a function of the ratio of donor polymer (PM6) and NFAs in PM6:IDIC and PM6:Y6 blend films, we conducted current density-voltage (*J*-*V*) characterization and external quantum efficiency (EQE) measurements, as shown in **Figure 1**. All data were collected using an inverted device architecture, with MoO_3 and ZnO as the hole and electron transport layers, respectively. Full details regarding device fabrication are provided in the Materials and Methods section in the supplementary information. The device *J*–*V* performance across the 1:1 to 5:1 ratio in both PM6:IDIC and PM6:Y6 are presented in Figure 1a,b. Both blends exhibited optimal performance at a D:A ratio of 1:1, with PM6:Y6 yielding a higher PCE than PM6:IDIC, consistent with previous reports.[22–25] As the acceptor content is decreased in both blend systems, we observed a rise in V_{OC}, accompanied by declines in J_{SC} and fill factor (FF). It is however noticeable that the decline in PCE with decreasing acceptor content is more pronounced for PM6:Y6 than PM6:IDIC, resulting in PM6:IDIC devices outperforming PM6:Y6 for D:A ratios of 3:1 or higher (see also Table S1, Supporting Information). These trends can be ascribed to a combination of morphology changes, alterations in energetics, and variations in charge carrier lifetimes, which we will elucidate further below.[11]

As illustrated in Figure 1c,d, device EQE's display a notable decline as the content of the PM6 donor increases, even within the absorption region of PM6. As such, the reductions in EQE cannot be assigned primarily to a lower light absorption but are due to a decrease in internal quantum efficiency. The EQE and current losses associated with a decreasing acceptor concentration (and thus an increasing donor content) are markedly more pronounced in devices employing Y6 than in those utilizing IDIC. Overall trends in device performance characteristics are summarized in Figure 1e. For both NFA's, lowering the PM6 donor content below 1:1 shows only relatively minor changes in performance compared to lower acceptor content devices, therefore we focus herein on low acceptor content in NFA devices; we also note low donor content devices have already been extensively studied in the literature.[26] As we discuss further below, we find that the loss of performance with lower acceptor content is correlated with a loss of acceptor aggregation, with this having the greatest impact on device performance for PM6:Y6 devices.

The EQE spectra shown in Figure 1c,d show distinct trends in the onset wavelength for IDIC and Y6 blends as a function of blend composition (see also Figure S2, Supporting Information).[27,28] In the case of IDIC blends, the onset, a measure of the acceptor optical bandgap, remains invariant,[28] whilst for Y6 blends, this onset blueshifts to higher energy with lower acceptor content. This blueshift for Y6 is consistent with previous reports of Y6's absorption onset shifting to longer wavelengths with increased aggregated/crystalline domains.[27,29] This blueshift therefore results from lower Y6 content which suppresses Y6 aggregation/crystallization, consistent with a reduced proportion of pure Y6 domains, and greater dominance of molecularly mixed PM6:Y6. In contrast, the absence of such spectral shifts for PM6:IDIC blends is consistent with the previously reported weaker charge transfer character and lower crystallinity of IDIC.[30] It is notable that the optical bandgap trends evidenced by these EQE data correlate with trends in V_{OC} (Figure 1e), with PM6:Y6 devices showing the most prominent increase in optical bandgap and the largest increase in V_{OC} with lower acceptor content.[16,28]

We turn now to GIWAXS analysis of the molecular packing structures within thin PM6:IDIC and PM6:Y6 blend films. As

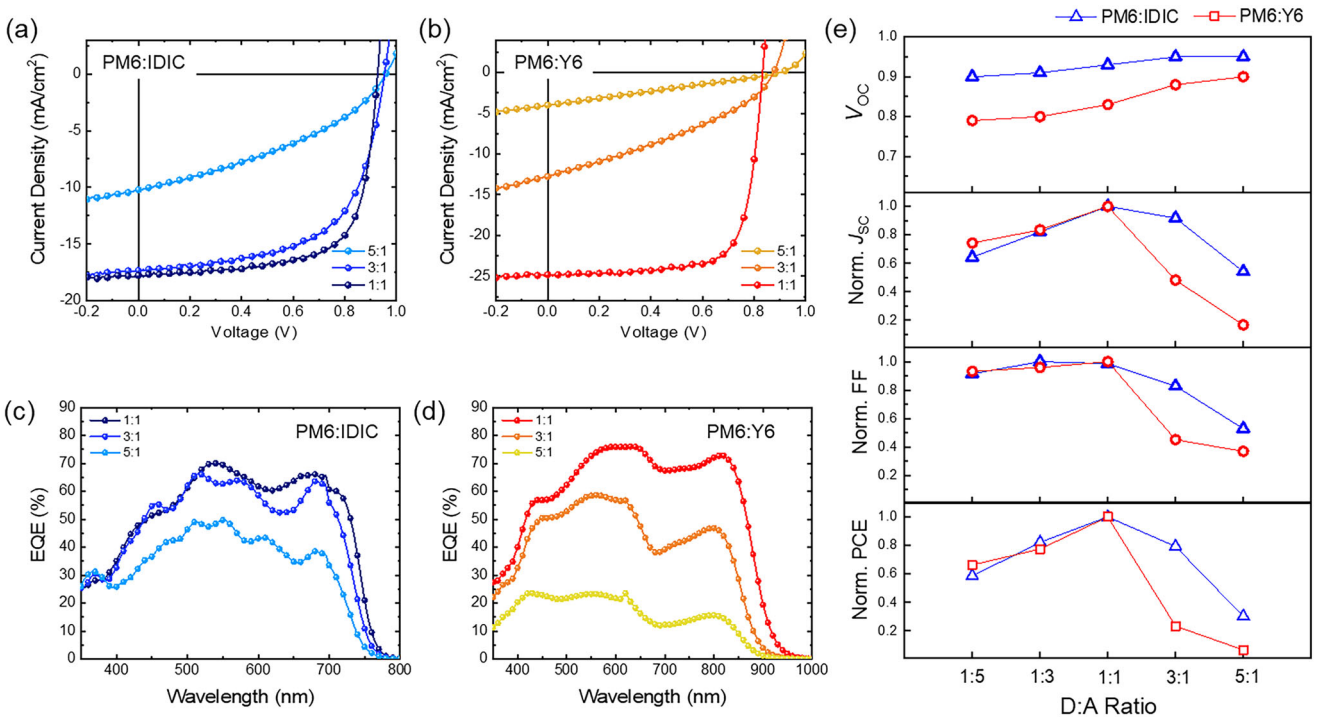

Figure 1. Device performance and electrical parameters comparison. *J–V* characteristics of a) PM6:IDIC and b) PM6:Y6 solar cells. EQE spectra of c) PM6:IDIC and d) PM6:Y6 solar cells. e) Comparison of device parameters (V_{OC}, J_{SC}, FF, and PCE) for PM6:IDIC and PM6:Y6 solar cell devices.

illustrated in the 2D diffraction patterns and the accompanying line cut profiles (Figures S3 and S4 and Table S3, Supporting Information), both neat NFAs exhibit a pronounced (010) diffraction peak at circa 1.8 $Å^{-1}$, reflecting a predominant face-on orientation, as well as π–π stacking peak at circa 1.7 $Å^{-1}$ in blend. It is notable that Y6 thin films exhibited stronger diffraction peaks than IDIC,[31] consistent with its previously reported higher crystallinity and stronger molecular interactions.[30] The PM6 polymer film shows a comparatively weaker, face-on arrangement. In the case of the blends, PM6:Y6 thin films primarily reflected the diffraction patterns of Y6, as observed in Figure S4 (Supporting Information). For both fullerene and NFAs, several studies have previously reported that reducing the acceptor content leads to a suppression of acceptor domain size[32–34] and crystallinity. Consistent with this conclusion, as the NFA content is reduced in PM6:Y6 blends, the intensity of the Y6 (010) peak decreases, whilst retaining a stronger face-on structure,[35] consistent with a suppression of crystalline Y6 domains in high donor content films. On the other hand, the 2D diffraction pattern for PM6:IDIC exhibits a weaker composition dependence. These GIWAXS data show that crystalline acceptor domains are present in 1:1 PM6:Y6 films but suppressed in films with lower Y6 content. In contrast, for IDIC, the formation of such crystalline domains is less significant even in the 1:1 blend films, consistent with its previously reported lower intermolecular interactions.[29,30,36]

UV–vis absorption (Figure S5, Supporting Information) and photoluminescence (PL) (**Figure** 2c,d) spectra were measured to determine the correlations between optical properties with morphological and device parameters. Both the absorption and PL data exhibit analogous trends in bandgap with blend composition to the EQE data discussed above; as the Y6 content is reduced, the absorption and PL onsets (reflecting the optical bandgap) blueshift by circa 50 meV, whilst for IDIC the absorption and PL onsets are rather invariant with blend composition. A higher IDIC LUMO energy level relative to Y6 has been reported in the literature from cyclic voltammetry analyses (Figure 2a).[37–39]

However, the associated higher IDIC optical bandgap also results in a lower solar light absorption (Figure 2b), contributing to the reduced J_{SC} and PCE for optimized PM6:IDIC solar cells (Figure 1). The PL spectra in Figure 2c show that PM6:IDIC blends exhibit more pronounced longer wavelength (≈900 nm) PL than neat IDIC. This corresponds to redshifted PL from interfacial charge transfer states in these blends, consistent with previous literature.[40] In contrast, no such pronounced longer wavelength PL is observed for PM6:Y6 blends (Figure 2d), consistent with the absence of coulombically bound, emissive interfacial charge transfer (CT) states in this blend.[41] The absence of such bound CT states has been suggested to be a key factor behind the high performance of PM6:Y6 solar cells.[42]

To investigate the charge generation and separation processes in PM6:IDIC and PM6:Y6 blends, ultrafast transient absorption spectroscopy (TAS) measurements were employed, as shown in **Figure** 3. The investigations focused on blend films within the spectral range of 850–1400 nm, employing NFA excitation at 700 nm to initiate the hole transfer process from NFA to PM6 (see also Figure S6, Supporting Information for the corresponding UV–vis region (400–800 nm) TAS spectra). In the PM6:IDIC (1:1) blend, depicted in Figure 3a, an initial photoinduced absorption (PIA) at ≈870 nm, assigned to IDIC excitons,[42] evolves within a few picoseconds to a redshifted absorption at ≈950 nm, assigned to CT / charge pair states. This rapid transition

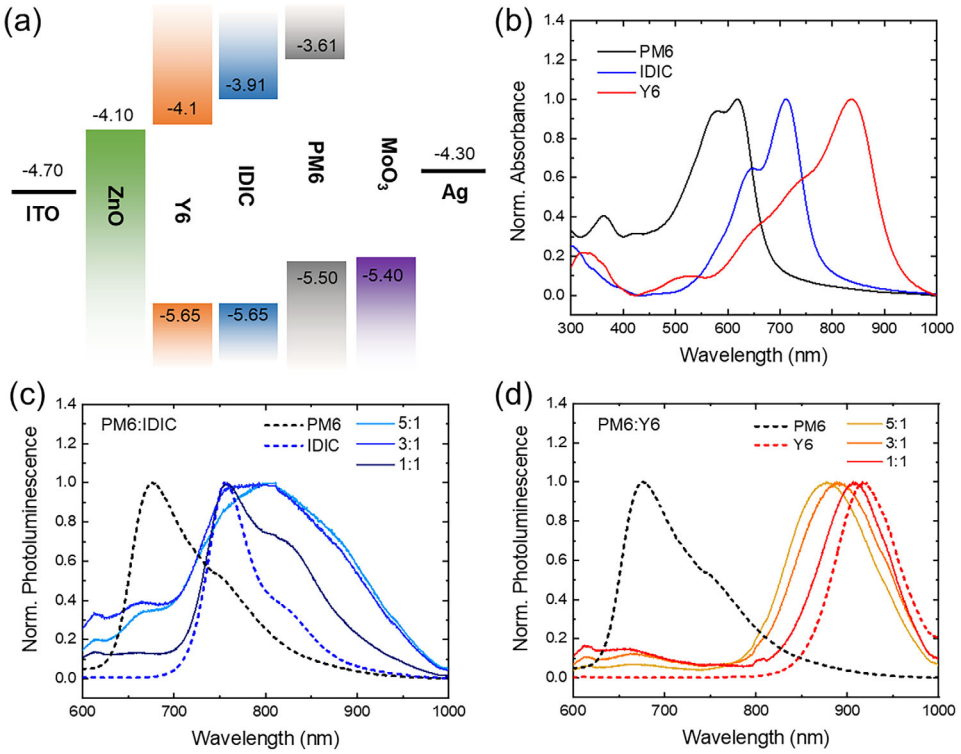

Figure 2. The energy level and study state optical analysis. a) Approximate electronic energy levels of the materials used in this work in thin films, obtained from the literature measured by cyclic voltammetry;[37–39] b) Normalized UV–vis absorption spectra for neat material films. Normalized PL spectra with 532 nm excitation wavelength of c) PM6:IDIC and d) PM6:Y6 films with varying D:A ratio, including neat materials.

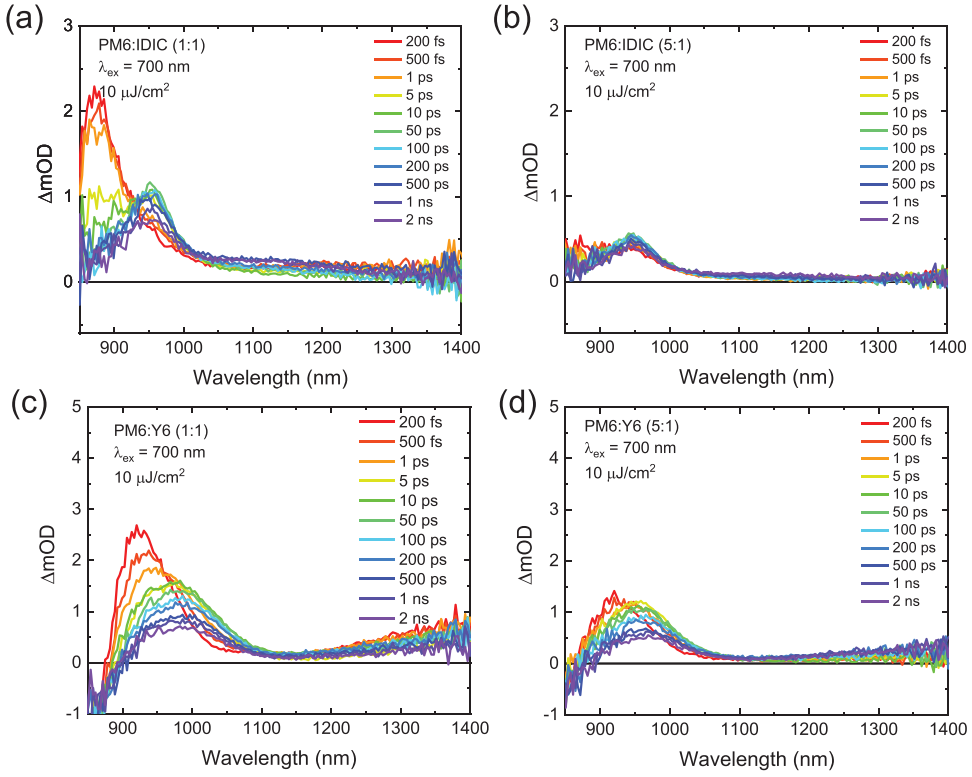

Figure 3. Ultrafast transient absorption study. Transient absorption spectra with respect to wavelength as a function of time delay for PM6:IDIC blends with a) 1:1 and b) 5:1 ratio and PM6:Y6 blends with c) 1:1 and d) 5:1 ratio excited at 700 nm, 10 μJ cm^{-2}.

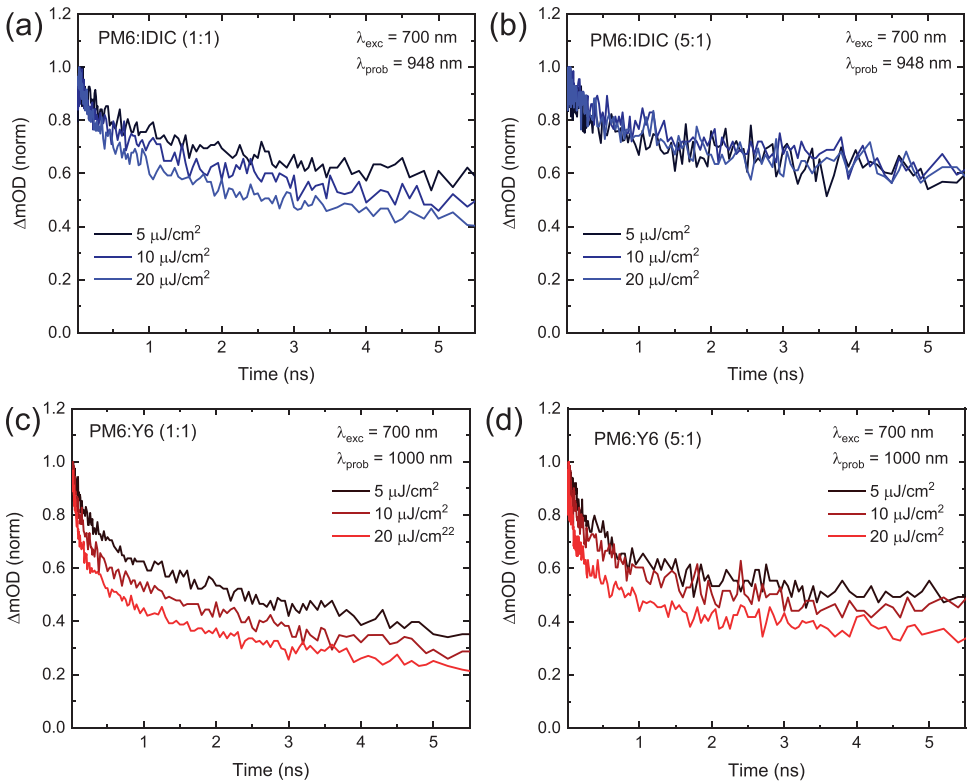

Figure 4. Kinetic response of ultrafast transient study. Pump fluence-dependent transient absorption traces of PM6:IDIC blends with a) 1:1 and b) 5:1 ratios excited at 700 nm, probed at 948 nm, and PM6:Y6 blends with c) 1:1 and d) 5:1 ratios excited at 700 nm, probed at 1000 nm. For both blend systems, the probe wavelengths correspond to CT/charge pair photoinduced absorption.

underscores an efficient exciton separation process. Likewise, for the 1:1 PM6:Y6 blend shown in Figure 3c, exciton PIA is initially detected at ≈920 nm and evolves into charge PIA state at ≈980 nm within a few picoseconds, consistent with previous literature.[41] We note Y6 excitons may also exhibit significant CT character,[43] although even in this case, charge separation still primarily occurs at PM6 / Y6 interfaces. For both 5:1 blends, only minor acceptor exciton PIA is observed, with the transient spectra already being dominated by CT / charge pair PIA from 200 fs (our instrument response), demonstrating exciton separation within our 200 fs instrument response. This is consistent with the 5:1 NFA content blends being dominated by molecularly mixed PM6:NFA domains, such that there is no exciton diffusion required for charge generation, and shows underlying hole transfer kinetics of <200 fs. Such ultrafast charge transfer demonstrates efficient charge generation in all the blends studied, showing that the trends in device performance trends in Figure 1 do not originate from trends in charge separation efficiency. We note that Y6 has the potential to form intermolecular charge transfer (ICT) excitons due to strong electronic coupling between Y6 molecules.[30,44] However, the contribution of ICT excitons generated within the pure Y6 domain to overall charge generation is expected to be minor compared to interfacial charge separation. The pronounced 920 nm excitonic signal in the PM6:Y6 1:1 blend suggests a greater presence of pure Y6 aggregated/crystalline domains[31] compared to the suppressed initial excitonic signal in the 5:1 blend. **Figure 4** depicts the decay dynamics of CT/charge pair photoinduced absorption in 1:1 and 5:1 blends as a function of excitation density. For the 1:1 PM6:IDIC blend, the decays are observed to accelerate with increasing laser intensity, indicating a dominance of the bimolecular recombination of separated charges. In contrast, the 5:1 PM6:IDIC blend exhibits intensity-independent kinetics, showing the dominance of monomolecular (i.e., geminate) recombination of bound interfacial CT states. This is consistent with the 5:1 blend exhibiting a more molecular mixed morphology, as discussed above; previous studies of other D:A blends have highlighted how the suppression of pure domains, and increased presence of molecular mixed domains, results in the greater dominance of monomolecular CT state recombination and suppression of bimolecular recombination.[40,45,46] Whilst ultrafast bimolecular recombination is a consequence of the high laser intensities employed in ultrafast-TAS studies, the observation of significant geminate (CT state), intensity-independent, recombination in the 5:1 blend is likely to be a significant factor behind the lower EQE and J_{SC}'s observed for the 5:1 PM6:IDIC blend. Analogous behavior is also observed for the PM6:Y6 blends, although significant intensity dependence of the decay kinetics is still observed in the 5:1 blend, reflecting less dominant geminate CT recombination, consistent with the absence of CT state photoluminescence (Figure 2). It is also noticeable that as monomolecular (CT state) recombination is less dominant for the 5:1 PM6:Y6 blend than the PM6:IDIC blend, differences in CT geminate recombination losses cannot explain the lower PCE of 5:1 PM6:Y6 solar cells. As such we now

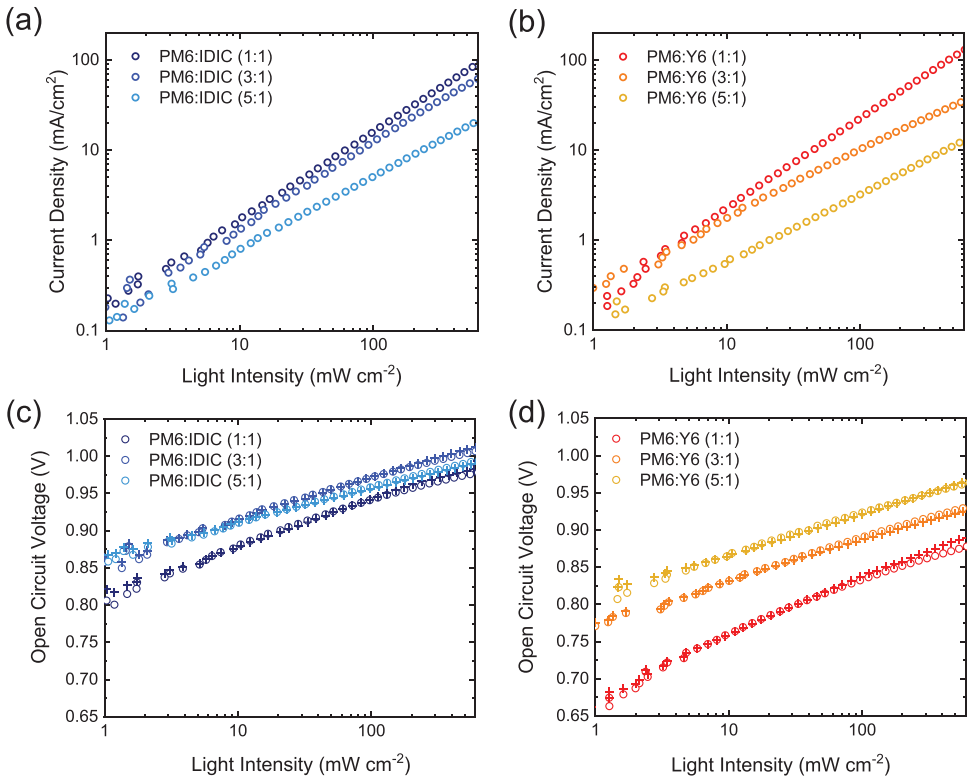

Figure 5. Intensity-dependent device analysis. Light intensity-dependent short circuit current of a) PM6:IDIC and b) PM6:Y6 solar cells with various D:A ratios. Light intensity-dependent open circuit voltage measured (circle) and reconstructed (cross)[47] of c) PM6:IDIC and d) PM6:Y6 solar cells with various D:A ratios blend.

turn to an analysis of the charge collection efficiencies of these devices.

In order to analyze charge collection efficiency, we consider first analyses of device performance as a function of light intensity. **Figure** 5a,b show log–log plots of J_{SC} versus light intensity for PM6:IDIC and PM6:Y6 devices respectively. These plots show the typical power law behavior, $J_{SC} \propto I^{\alpha}$, where α corresponds to the gradient of these log:log plots. $\alpha = 1$ corresponds to the absence of non-linear losses, and therefore the absence of bimolecular recombination losses during charge collection. The presence of bimolecular losses limiting short circuit collection efficiency results in gradients α <1.[48] For the PM6:IDIC (1:1 and 3:1) devices, the gradients approach unity (α = 0.96 and 0.94), indicating only minor bimolecular recombination within this device at a short circuit. For the 5:1 device, a lower gradient was observed (α of 0.80), reflecting bimolecular loss-dominated charge collection, consistent with its more molecularly mixed nanomorphology. In contrast, whilst the 1:1 PM6:Y6-based device exhibits a unity gradient of $\alpha = 1.0$, showing negligible bimolecular recombination losses during extraction, this gradient is substantially lowered as the NFA content is lowered, with α = 0.76 and 0.73 for 3:1 and 5:1 respectively (see also Figure S7, Supporting Information for current linearity with respect to light intensity). These results indicate that whilst the 1:1 PM6:Y6 device has a near-unity collection efficiency, this collection efficiency is substantially degraded as the Y6 content is lowered, consistent with the J_{SC} and EQE data trends in Figure 1. These data thus indicate that the primary reason for device PCE drops off with lower NFA content is more severe for PM6:Y6 devices than PM6:IDIC devices due to a more significant drop off in charge collection efficiency.

Charge extraction (CE) and transient photovoltage (TPV) measurements were undertaken on the device studied to determine the underlying charge carrier energetics, mobilities, and bimolecular recombination kinetics.[49] The average charge carrier densities (n) of the active layer at an open circuit, obtained from CE measurements as a function of V_{OC}, are depicted in **Figure** 6a,b. At open circuits in organic solar cells, V_{OC} primarily corresponds to the quasi-Fermi level splitting within the photoactive layer, as such plots of n versus V_{OC} serve as an in situ assay of the effective electronic bandgap of the blend. It is clearly noticeable that for PM6:IDIC devices n versus V_{OC} are almost independent of blend composition, showing that the blend electronic bandgap is independent of blend composition. This is consistent with our observation above the optical bandgap of these IDIC blends was also independent of blend composition, attributed to relatively weak electronic interactions between IDIC molecules even in aggregated IDIC domains. In contrast, the PM6:Y6 devices, as shown in Figure 6b, the relationship between n and V_{OC} is strongly composition-dependent, with V_{OC} at a given charge density decreasing with increasing Y6 content. At matched charge densities, the measured V_{OC} is reduced with increased Y6 content, indicative of a substantial reduction by ~ 250 meV in electronic bandgap. In contrast for PM6:IDIC devices, the equivalent reduction in electronic bandgap is <50 meV. It can thus be concluded that increased dominance of pure aggregated/crystalline

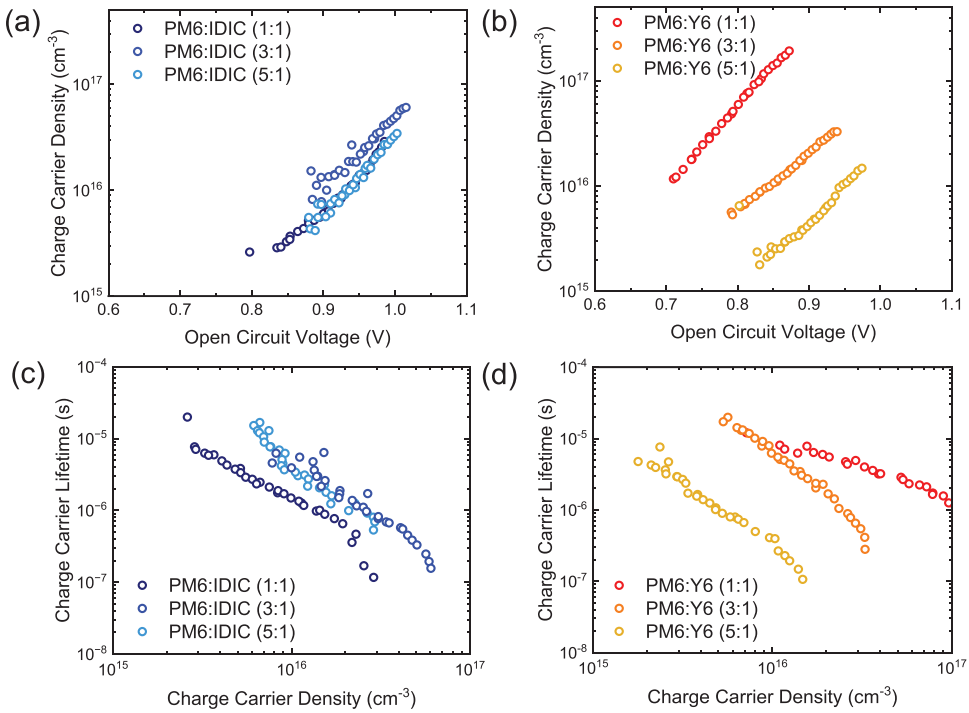

Figure 6. Charge carrier density and lifetime study in devices at open circuit voltage. Charge extraction data as a function of light intensity allow determination of charge density versus open circuit voltage, as plotted for a) PM6:IDIC and b) PM6:Y6 solar cells for different D:A ratios. Charge carrier lifetime versus charge carrier density determined from charge extraction and transient photovoltage measurements for different donor-acceptor ratios for c) PM6:IDIC and d) PM6:Y6 solar cells.

Y6 domains with increasing Y6 content in PM6/Y6 devices results in a ≈250 meV reduction in the electronic bandgap of these devices.

Figure 6c,d plots charge carrier lifetimes determined from transient photovoltage decays versus the carrier densities determined from charge extraction data, both measured at open circuit as a function of light intensity. We note the excitation conditions employed in these TPV measurements result in charge carrier densities comparable to solar irradiation, in contrast to the pulsed excitation conditions employed in our TAS above, and thus yield much longer, and device-operation relevant, carrier lifetimes. For the PM6:IDIC devices, these charge carrier lifetimes are rather independent of blend composition (being slightly slower recombination for the 3:1 and 5:1 blends). In contrast, the charge carrier lifetimes in PM6:Y6 devices are strongly charge density-dependent, exhibiting much slower recombination at matched charge densities as the Y6 content is increased. This observation indicates that increasing the Y6 content from 5:1 to 1:1 results in a significant (≈10 fold) reduction in bimolecular recombination. Reconstructed V_{OC}'s, determined from these charge density and recombination data versus device J_{SC} were found to be in excellent agreement with directly measured V_{OC}'s (Figure 5c,d), confirming the validity of these data. Average effective mobility for electrons and holes determined from charge extraction at short circuit (Figure S8, Supporting Information),[50,51] indicate that whilst average charge mobilities for PM6:IDIC devices are essentially independent of blend composition, for PM6:Y6 devices charge carrier mobilities increase with increasing acceptor content. Charge collection efficiency in organic solar cells is primarily determined by kinetic competition between charge transport, determined by drift mobilities, and charge density-dependent bimolecular recombination. For PM6:IDIC devices, both charge mobility and bimolecular recombination are rather independent of blend composition, resulting in charge collection efficiency being relatively independent of blend composition. However, for PM6:Y6 devices, lowering the Y6 content results in an acceleration of bimolecular recombination and reduction of carrier mobility, leading to a rapid drop off in collection efficiency (we note that space charge limitations may also impact on the photocurrent densities for low Y6 content devices, see Figure S9, Supporting Information).[52,53] This acceleration of sharp drop off's of EQE, FF, and J_{SC} with decreasing Y6 content in PM6:Y6 devices is shown in Figure 1.

The reduction in electronic bandgap with increasing Y6 content in PM6:Y6 devices determined from our charge extraction data is particularly striking. It is analogous to that reported previously for P3HT:PCBM devices,[11] and assigned, as previously, to acceptor aggregation/crystallization, as supported by our morphology data discussed above. This reduction in electronic bandgap is the origin of the decrease in device V_{OC} from 5:1 to 1:1, although as highlighted above, this effect is partially mitigated by the increase in carrier lifetimes with increasing Y6 content, as discussed further below. This reduction in electronic bandgap can be assigned to a lowering of the Y6 LUMO level with Y6 aggregation, consistent with the corresponding reduction in optical bandgap, it results in a ≈250 meV LUMO level electronic offset between molecular mixed PM6/Y6 and aggregated / crystalline Y6 domains.

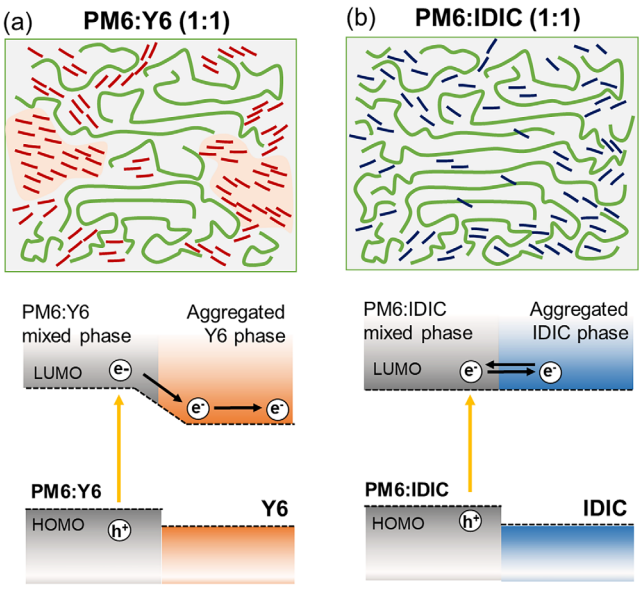

Figure 7. Illustration of the proposed model for NFA-based bulk-heterojunction film. a) Spatial separation of electrons and holes are assisted by localization of electrons in aggregated crystalline Y6 domains, driven by a Y6 LUMO level energetic offset between mixed and pure domains. b) Weaker IDIC electronic interactions result in the absence of a significant energetic offset between mixed and pure domains. The green long lines indicate PM6, and small red and blue line segments indicate Y6 and IDIC molecules respectively.

Figure 7 summarizes our understanding of the role of Y6 aggregation/crystallization in suppressing bimolecular recombination in optimized PM6:Y6 devices. Strong electronic interactions between Y6 molecules in pure domains result in smaller optical and, in particular, electronic bandgaps and thus a lower LUMO level. The resulting LUMO energetic offset between the mixed PM6:Y6 and aggregated Y6 domains serves as an energetic offset to spatially localize photogenerated electrons in pure Y6 domains, increasing the spatial separation of these electrons and from PM6 holes, thus suppressing bimolecular recombination. This results in the recombination becoming more "non-Langevin" (we note that the charge carrier mobilities increase with increasing Y6 content, so cannot explain the slower recombination). This retardation of recombination kinetics is the dominant reason for the significant increases in device FF, J_{SC}, and PCE as the Y6 content is increased from 5:1 to 1:1. In contrast, the absence of a significant LUMO energetic offset between mixed PM6:IDIC and aggregated IDIC domains results in the weaker composition dependence of PM6:IDIC device performance highlighted above. We have previously reported that Y6's high quadrupole moment suppresses recombination in PM6:Y6 bilayer devices.[15] As such, the stronger electronic interactions between Y6 molecules compared to IDIC are likely to result, at least in part, from Y6's higher molecular quadrupole moment,[17] with this high quadrupole moment contributing to the energetic offset between mixed and pure domains we observe herein. It is striking that the LUMO energetic offset we report herein between mixed and pure Y6 domains, and its impact on bimolecular recombination kinetics, is very similar to that we have previously proposed for the most successful fullerene acceptor, PCBM.[11] We have also reported evidence for an analogous offset with the wider bandgap NFA, IDTBR.[54] This energetic offset has the downside of reducing V_{OC} as it lowers the device electronic bandgap. However, it is apparent that this downside is outweighed by its beneficial effect in aiding the spatial separation of charges, and thereby suppressing bimolecular recombination losses, increasing device J_{SC} and *FF*, as well as mitigating the reduction in V_{OC}. It thus appears that this energetic offset between mixed and pure domains is a key design requirement for both high-performance fullerene and non-fullerene electron acceptors in organic solar cells.

3. Conclusion

Several key features have been identified as critical to the high performance of PM6:Y6 BHJ organic solar cells. These include the long exciton lifetime of Y6,[55] low energetic disorder,[41] and the absence of bound interfacial charge transfer states.[56,57] The study herein suggests an additional feature of this system is critical to its high performance. LUMO level energetic offset between mixed PM6:Y6 and pure Y6 domains which aids the spatial separation of electron and holes, thereby suppressing recombination losses in the photoactive BHJ. This energetic offset results from strong electronic interactions between Y6 molecules in pure Y6 domains, including those resulting from its high quadrupole moment. This LUMO energetic offset between mixed and pure domains highlighted for Y6 herein is analogous to that we have previously reported for BHJ employing the fullerene acceptor PCBM.[11] As such this study highlights both the importance of BHJ nanomorphology, and in particular the presence of not only mixed but pure domains in high-performance NFA bases OPV devices, and in particular the design requirement for efficient fullerene and non-fullerene acceptors that pure acceptor domains should exhibit a larger electron affinity than the acceptor dispersed in mixed donor/acceptor domains. This larger electron affinity, resulting from acceptor/acceptor molecular interactions in the pure acceptor domains, stabilizes electrons in these domains, thereby suppressing recombination losses and enhancing device performance.

Supporting Information

Supporting Information is available from the Wiley Online Library or from the author.

Acknowledgements

S.J. and A.R. contributed equally to this work. The authors thank the Heeger Center for Advanced Materials (HCAM), Research Institute for Solar and Sustainable Energies (RISE), and the Gwangju Institute of Science Technology (GIST)-Imperial College London (ICL) international collaboration R&D Centre for help with device fabrication and measurements. This research was supported by the Global Research Laboratory Program (NRF-2017K1A1A2013153), and Postdoctoral Fellowship Program (Nurturing Next-generation Researchers, NRF-2021R1A6A3A03045866) of the National Research Foundation (NRF) funded by the Ministry of Science, ICT and Future Planning, Korea, and also by the UK's EPSRC funded project ATIP EP/T028513/1. The authors also like to thank Richard A. Pacalaj for his helpful comments and valuable insights to this work.

Conflict of Interest

The authors declare no conflict of interest.

Data Availability Statement

The data supporting the findings of this study are available from the corresponding authors upon request.

Keywords

bulk heterojunction, charge transfer, intermixed phases, non-fullerene acceptors, photovoltaic device, recombination dynamics, solar cells

Received: March 23, 2025
Revised: June 1, 2025
Published online:

[1] J. Fu, P. W. K. Fong, H. Liu, C. S. Huang, X. Lu, S. Lu, M. Abdelsamie, T. Kodalle, C. M. Sutter-Fella, Y. Yang, G. Li, *Nat. Commun.* **2023**, *14*, 1760.
[2] L. Zhu, M. Zhang, J. Xu, C. Li, J. Yan, G. Zhou, W. Zhong, T. Hao, J. Song, X. Xue, Z. Zhou, R. Zeng, H. Zhu, C. C. Chen, R. C. I. MacKenzie, Y. Zou, J. Nelson, Y. Zhang, Y. Sun, F. Liu, *Nat. Mater.* **2022**, *21*, 656.
[3] X. Li, Q. Zhang, J. Yu, Y. Xu, R. Zhang, C. Wang, H. Zhang, S. Fabiano, X. Liu, J. Hou, F. Gao, M. Fahlman, *Nat. Commun.* **2022**, *13*, 2046.
[4] H. Chen, Y. Huang, R. Zhang, H. Mou, J. Ding, J. Zhou, Z. Wang, H. Li, W. Chen, J. Zhu, Q. Cheng, H. Gu, X. Wu, T. Zhang, Y. Wang, H. Zhu, Z. Xie, F. Gao, Y. Li, Y. Li, *Nat. Mater.* **2025**, *24*, 444.
[5] Y. Jiang, S. Sun, R. Xu, F. Liu, X. Miao, G. Ran, K. Liu, Y. Yi, W. Zhang, X. Zhu, *Nat. Energy* **2024**, *9*, 975.
[6] J. Wang, Z. Zheng, P. Bi, Z. Chen, Y. Wang, X. Liu, S. Zhang, X. Hao, M. Zhang, Y. Li, J. Hou, *Natl. Sci. Rev.* **2023**, *10*, nwad085.
[7] J. Yuan, Y. Zou, *Org. Electron.* **2022**, *102*, 106436.
[8] C. Cheng, S. Wong, G. Lecroy, S. Schneider, E. Gomez, M. F. Toney, A. Salleo, C. Cheng, G. Lecroy, A. Salleo, S. Wong, E. Gomez, S. Schneider, M. F. Toney, *Adv. Energy Mater.* **2023**, *13*, 2204297.
[9] J. Song, M. Zhang, T. Hao, J. Yan, L. Zhu, G. Zhou, R. Zeng, W. Zhong, J. Xu, Z. Zhou, X. Xue, C.-C. Chen, W. Tang, H. Zhu, Z. Ma, Z. Tang, Y. Zhang, F. Liu, *Research* **2022**, *2022*, 9817267.
[10] A. Melianas, V. Pranculis, D. Spoltore, J. Benduhn, O. Inganäs, V. Gulbinas, K. Vandewal, M. Kemerink, A. Melianas, O. Inganäs, M. Kemerink, V. Pranculis, V. Gulbinas, D. Spoltore, J. Benduhn, K. Vandewal, *Adv. Energy Mater.* **2017**, *7*, 1700888.
[11] F. C. Jamieson, E. B. Domingo, T. McCarthy-Ward, M. Heeney, N. Stingelin, J. R. Durrant, *Chem. Sci.* **2012**, *3*, 485.
[12] W. Li, S. Zeiske, O. J. Sandberg, D. B. Riley, P. Meredith, A. Armin, *Energy Environ. Sci.* **2021**, *14*, 6484.
[13] D. Li, X. Zhang, D. Liu, T. Wang, *J. Mater. Chem. A* **2020**, *8*, 15607.
[14] M. Kim, S. U. Ryu, S. A. Park, Y. J. Pu, T. Park, *Chem. Sci.* **2021**, *12*, 14004.
[15] Y. Fu, T. H. Lee, Y. C. Chin, R. A. Pacalaj, C. Labanti, S. Y. Park, Y. Dong, H. W. Cho, J. Y. Kim, D. Minami, J. R. Durrant, J. S. Kim, *Nat. Commun.* **2023**, *14*, 1870.
[16] N. Yao, Y. Xia, Y. Liu, S. Chen, M. P. Jonsson, F. Zhang, *ACS Appl. Energy Mater.* **2021**, *4*, 14335.
[17] S. Y. Park, C. Labanti, R. A. Pacalaj, T. H. Lee, Y. Dong, Y. C. Chin, J. Luke, G. Ryu, D. Minami, S. Yun, J. Il Park, F. Fang, K. B. Park, J. R. Durrant, J. S. Kim, *Adv. Mater.* **2023**, *35*, 2306655.
[18] J. Luke, E. J. Yang, Y.-C. Chin, Y. Che, L. Winkler, D. Whatling, C. Labanti, S. Y. Park, J.-S. Kim, *Adv. Energy Mater.* **2022**, *12*, 2201267.
[19] M. B. Price, P. A. Hume, A. Ilina, I. Wagner, R. R. Tamming, K. E. Thorn, W. Jiao, A. Goldingay, P. J. Conaghan, G. Lakhwani, N. J. L. K. Davis, Y. Wang, P. Xue, H. Lu, K. Chen, X. Zhan, J. M. Hodgkiss, *Nat. Commun.* **2022**, *13*, 2827.
[20] S. Chandrabose, K. Chen, A. J. Barker, J. J. Sutton, S. K. K. Prasad, J. Zhu, J. Zhou, K. C. Gordon, Z. Xie, X. Zhan, J. M. Hodgkiss, *J. Am. Chem. Soc.* **2019**, *141*, 6922.
[21] Y. Firdaus, V. M. Le Corre, S. Karuthedath, W. Liu, A. Markina, W. Huang, S. Chattopadhyay, M. M. Nahid, M. I. Nugraha, Y. Lin, A. Seitkhan, A. Basu, W. Zhang, I. McCulloch, H. Ade, J. Labram, F. Laquai, D. Andrienko, L. J. A. Koster, T. D. Anthopoulos, *Nat. Commun.* **2020**, *11*, 5220.
[22] J. Hou, O. Inganas, R. H. Friend, F. Gao, *Nat. Mater.* **2018**, *17*, 119.
[23] Z. Cao, Q. Liao, Z. Zhang, T. Huang, Z. Deng, H. Guan, S. Geng, D. Wang, J. Zhang, *Dyes Pigm.* **2023**, *219*, 111493.
[24] Z. C. Wen, H. Yin, X. T. Hao, *Surf. Interfaces* **2021**, *23*, 100921.
[25] R. Yu, G. Wu, Z. Tan, *J. Energy Chem.* **2021**, *61*, 29.
[26] N. Yao, J. Wang, Z. Chen, Q. Bian, Y. Xia, R. Zhang, J. Zhang, L. Qin, H. Zhu, Y. Zhang, F. Zhang, *J. Phys. Chem. Lett.* **2021**, *12*, 5039.
[27] P. Wan, X. Chen, Q. Liu, S. Mahadevan, M. Guo, J. Qiu, X. Sun, S.-W. Tsang, M. Zhang, Y. Li, S. Chen, *J. Phys. Chem. Lett.* **2021**, *12*, 10595.
[28] X. Chen, B. Kan, Y. Kan, M. Zhang, S. Byeok Jo, K. Gao, F. Lin, F. Liu, X. Peng, Y. Cao, A. K.-Y. Jen, X. Chen, B. Kan, Y. Kan, S. B. Jo, K. Gao, A. K.-Y. Jen, X. B. Peng, Y. Cao, M. Zhang, F. Liu, F. Lin, *Adv. Funct. Mater.* **2020**, *30*, 1909535.
[29] Y. Xiao, J. Yuan, G. Zhou, K. C. Ngan, X. Xia, J. Zhu, Y. Zou, N. Zhao, X. Zhan, X. Lu, *J. Mater. Chem. A* **2021**, *9*, 17030.
[30] S. Mahadevan, T. Liu, S. M. Pratik, Y. Li, H. Y. Ho, S. Ouyang, X. Lu, H. L. Yip, P. C. Y. Chow, J. L. Brédas, V. Coropceanu, S. K. So, S. W. Tsang, *Nat. Commun.* **2024**, *15*, 2393.
[31] X. Xia, L. Mei, C. He, Z. Chen, N. Yao, M. Qin, R. Sun, Z. Zhang, Y. Pan, Y. Xiao, Y. Lin, J. Min, F. Zhang, H. Zhu, J. L. Bredas, H. Chen, X. K. Chen, X. Lu, *J. Mater. Chem. A* **2023**, *11*, 21895.
[32] M. Piralaee, A. Asgari, *Opt. Quantum Electron.* **2023**, *55*, 802.
[33] Z. Wen, X. Ma, X. Yang, P. Bi, M. Niu, K. Zhang, L. Feng, X. Hao, *Chin. Chem. Lett.* **2019**, *30*, 995.
[34] Z. Hamid, A. Wadsworth, E. Rezasoltani, S. Holliday, M. Azzouzi, M. Neophytou, A. A. Y. Guilbert, Y. Dong, M. S. Little, S. Mukherjee, A. A. Herzing, H. Bristow, R. J. Kline, D. M. DeLongchamp, A. A. Bakulin, J. R. Durrant, J. Nelson, I. McCulloch, *Adv. Energy Mater.* **2020**, *10*, 1903248.
[35] S. McAnally, H. Jin, R. Chu, N. Mallo, X. Wang, P. L. Burn, I. R. Gentle, P. E. Shaw, *ACS Appl. Mater. Interfaces* **2024**, *16*, 28958.
[36] D. Kroh, F. Eller, K. Schötz, S. Wedler, L. Perdigón-Toro, G. Freychet, Q. Wei, M. Dörr, D. Jones, Y. Zou, E. M. Herzig, D. Neher, A. Köhler, *Adv. Funct. Mater.* **2022**, *32*, 2205711.
[37] J. Yuan, Y. Zhang, L. Zhou, G. Zhang, H. L. Yip, T. K. Lau, X. Lu, C. Zhu, H. Peng, P. A. Johnson, M. Leclerc, Y. Cao, J. Ulanski, Y. Li, Y. Zou, *Joule* **2019**, *3*, 1140.
[38] Q. Fan, Y. Wang, M. Zhang, B. Wu, X. Guo, Y. Jiang, W. Li, B. Guo, C. Ye, W. Su, J. Fang, X. Ou, F. Liu, Z. Wei, T. Chien Sum, T. P. Russell, Y. Li, *Adv. Mater.* **2018**, *30*, 1704546.
[39] J. Bertrandie, J. Han, C. S. P. De Castro, E. Yengel, J. Gorenflot, T. Anthopoulos, F. Laquai, A. Sharma, D. Baran, *Adv. Mater.* **2022**, *34*, 2202575.
[40] S. D. Dimitrov, M. Azzouzi, J. Wu, J. Yao, Y. Dong, P. S. Tuladhar, B. C. Schroeder, E. R. Bittner, I. McCulloch, J. Nelson, J. R. Durrant, *J. Am. Chem. Soc.* **2019**, *141*, 4634.
[41] J. Wu, J. Lee, Y. C. Chin, H. Yao, H. Cha, J. Luke, J. Hou, J. S. Kim, J. R. Durrant, *Energy Environ. Sci.* **2020**, *13*, 2422.
[42] H. Cha, Y. Zheng, Y. Dong, H. Hwi Lee, J. Wu, H. Bristow, J. Zhang, H. K. Hin Lee, W. C. Tsoi, A. A. Bakulin, I. McCulloch, J. R. Durrant, *Adv. Energy Mater.* **2020**, *10*, 2001149.
[43] S. Shoaee, H. M. Luong, J. Song, Y. Zou, T. Q. Nguyen, D. Neher, *Adv. Mater.* **2024**, *36*, 2302005.

[44] R. Wang, C. Zhang, Q. Li, Z. Zhang, X. Wang, M. Xiao, *J. Am. Chem. Soc.* **2020**, *142*, 12751.
[45] E. Collado-Fregoso, S. N. Pugliese, M. Wojcik, J. Benduhn, E. Bar-Or, L. P. Toro, U. Hörmann, D. Spoltore, K. Vandewal, J. M. Hodgkiss, D. Neher, *J. Am. Chem. Soc.* **2019**, *141*, 2329.
[46] E. Collado-Fregoso, S. N. Hood, S. Shoaee, B. C. Schroeder, I. McCulloch, I. Kassal, D. Neher, J. R. Durrant, *J. Phys. Chem. Lett.* **2017**, *8*, 4061.
[47] S. Jeong, A. Rana, J. H. Kim, D. Qian, K. Park, J. H. Jang, J. Luke, S. Kwon, J. Kim, P. S. Tuladhar, J. S. Kim, K. Lee, J. R. Durrant, H. Kang, *Adv. Sci.* **2023**, *10*, 2206802.
[48] A. Rana, S. Y. Park, C. Labanti, F. Fang, S. Yun, Y. Dong, E. J. Yang, D. Nodari, N. Gasparini, J. Park, J. Shin, D. Minami, K. B. Park, J. S. Kim, J. R. Durrant, *Nat. Commun.* **2024**, *15*, 5058.
[49] S. Wheeler, D. Bryant, J. Troughton, T. Kirchartz, T. Watson, J. Nelson, J. R. Durrant, *J. Phys. Chem. C* **2017**, *121*, 13496.
[50] C. G. Shuttle, B. O'Regan, A. M. Ballantyne, J. Nelson, D. D. C. Bradley, J. De Mello, J. R. Durrant, *Appl. Phys. Lett.* **2008**, *92*, 93311.
[51] C. G. Shuttle, A. Maurano, R. Hamilton, B. O'Regan, J. C. De Mello, J. R. Durrant, *Appl. Phys. Lett.* **2008**, *93*, 183501.
[52] L. J. A. Koster, V. D. Mihailetchi, H. Xie, P. W. M. Blom, *Appl. Phys. Lett.* **2005**, *87*, 203502.
[53] A. Rana, A. Kumar, S. Chand, R. K. Singh, *J. Appl. Phys.* **2019**, *125*, 53102.
[54] H. Cha, G. Fish, J. Luke, A. Alraddadi, H. H. Lee, W. Zhang, Y. Dong, S. Limbu, A. Wadsworth, I. P. Maria, L. Francàs, H. L. Sou, T. Du, J. S. Kim, M. A. McLachlan, I. McCulloch, J. R. Durrant, *Adv. Energy Mater.* **2019**, *9*, 1901254.
[55] A. Classen, C. L. Chochos, L. Lüer, V. G. Gregoriou, J. Wortmann, A. Osvet, K. Forberich, I. McCulloch, T. Heumüller, C. J. Brabec, *Nat. Energy* **2020**, *5*, 711.
[56] S. M. Pratik, G. Kupgan, J. L. Brédas, V. Coropceanu, *Energy Environ. Sci.* **2025**, *18*, 841.
[57] L. Perdigón-Toro, H. Zhang, A. Markina, J. Yuan, S. M. Hosseini, C. M. Wolff, G. Zuo, M. Stolterfoht, Y. Zou, F. Gao, D. Andrienko, S. Shoaee, D. Neher, *Adv. Mater.* **2020**, *32*, 1906763.